Phytomedicine 141 (2025) 156721

Contents lists available at ScienceDirect

Phytomedicine

journal homepage: www.elsevier.com/locate/phymed

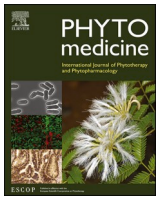

Original Article

Zengmian Yiliu formula suppresses cell cycle in immune-rich ovarian cancer patient-derived organoids

Qi Cao [a,1], Chunhui Cai [b,1], Chen Wang [b], Lanyang Li [b], Jiping Liu [b], Jian Zhang [b], Mingjie Rong [b], Jiaqi Ren [b], Yanyan Han [b], Jie Zhang [c,*], Xinxin Han [b,d,**]

[a] Obstetrics & Gynecology Hospital of Fudan University, Shanghai, China
[b] Shanghai LiSheng Biotech, Shanghai, China
[c] LongHua Hospital, Shanghai University of Traditional Chinese Medicine, 725 Wanping South Road, Xuhui District, Shanghai, China
[d] Organ Regeneration X Lab, LiSheng East China Institute of Biotechnology, Peking University, Jiangsu, China

ARTICLE INFO

Keywords:
Ovarian cancer
Cancer organoid
Zengmian Yiliu formula
Immune response gene
Cell cycle
Immune therapy

ABSTRACT

Background: Ovarian cancer, often diagnosed at advanced stages, has a 5-year survival rate below 50%, indicating a critical need for innovative treatments. The Zengmian Yiliu (ZMYL) formula, a Traditional Chinese Medicine (TCM) prescription, has shown potential in enhancing chemotherapy efficacy and improving patients' quality of life,

Purpose: To investigate the effects of the ZMYL formula on ovarian cancer organoids, focusing on its impact on organoid phenotypes and underlying mechanisms, and to explore its potential as an immunotherapeutic agent.

Methods: Ovarian cancer organoids were established from surgical tissues and treated with the ZMYL formula at varying concentrations. Network pharmacology was utilized to predict the formula's therapeutic targets and pathways, and molecular docking was conducted to validate ingredient-target interactions. Phenotypic changes were monitored, and RNA sequencing was performed post-treatment to analyze gene expression alterations.

Results: A total of 34 overlapping targets of 10 compounds in the ZMYL formula and ovarian cancer were predicted by Network pharmacology analysis. The ZMYL formula induced dose-dependent morphological changes in organoids, including a reduction in size and structural sparsity at higher concentrations. RNA sequencing revealed significant modulation of cell cycle and immune response pathways, with a particular focus on immunomodulatory effects. The formula's treatment targeted key genes involved in these processes, reshaping the tumor's molecular landscape.

Conclusions: This study establishes ZMYL's capacity to simultaneously target oncogenic drivers (e.g., cell cycle regulators) and immune checkpoints (e.g., CXCL10-mediated T cell recruitment) in ovarian cancer organoids. Unlike conventional monotherapy-focused approaches, ZMYL's multi-component mechanism offers a synergistic framework for integrating TCM with modern immunotherapies. These findings provide a foundation for future clinical evaluation of ZMYL as a precision medicine strategy to enhance treatment efficacy and mitigate chemoresistance in ovarian cancer.

Introduction

Ovarian cancer is a diverse disease with distinct histologic subtypes, each with unique risk factors and treatments; global estimates for 2020 identify over 133,000 new serous cases, highlighting the need for targeted prevention strategies (Wang et al., 2024a). Typically diagnosed at advanced stages due to late detection and chemotherapy resistance, it has a disheartening 5-year survival rate of less than 50%, emphasizing the pressing need for innovative therapeutic strategies (Bray et al., 2024). Recent research has begun to unravel the complex tumor microenvironment in ovarian cancer, revealing a landscape ripe for immunotherapeutic intervention (Luo et al., 2024). With the identification of key immunological markers and the role of homologous recombination deficiency in shaping the tumor microenvironment

* Corresponding author.
** Corresponding author at: Shanghai LiSheng Biotech, Shanghai, China.
E-mail addresses: zhangjie1122@shutcm.edu.cn (J. Zhang), xxhan@sibs.ac.cn (X. Han).
[1] These authors contributed equally to this work.

https://doi.org/10.1016/j.phymed.2025.156721
Received 10 October 2024; Received in revised form 18 March 2025; Accepted 1 April 2025
Available online 3 April 2025

(Vazquez-Garcia et al., 2022), the path forward includes the development of targeted therapies that harness the immune system to combat this deadly disease.

Building on the quest for innovative therapeutic approaches for ovarian cancer, Traditional Chinese Medicine (TCM) offers a promising avenue. The Zengmian Yiliu (ZMYL) formula, an empirical prescription adapted from the ancient Baozhen Decotion, has demonstrated potential in complementing conventional treatments (Gong et al., 2015a; Qi et al., 2012). Comprising 10 herbs with properties that nourish Qi and Yin, as well as clear heat and detoxify, the ZMYL formula has been clinically shown to enhance chemotherapy efficacy, mitigate its side effects, and notably improve the quality of life for patients. Notably, studies have reported a higher survival rate and better Karnofsky Performance Status (KPS) in patients administered the ZMYL formula compared to chemotherapy alone (Gong et al., 2015b; Zhang et al., 2015). The formula's multifaceted action on tumor cell apoptosis suggests a role in regulating cellular death mechanisms (Qi et al., 2012). Despite these promising findings, the intricate "multi-components and multi-targets" nature of TCM like the ZMYL formula necessitates further exploration to elucidate its precise mechanisms, especially in the context of immunotherapy, offering a bridge between traditional practices and modern medical advancements.

Given the intricate and prolonged clinical effects of Traditional Chinese Medicine (TCM), such as the ZMYL formula, and the challenges in deciphering their downstream mechanisms, an *in vitro* model that replicates the human tumor microenvironment is essential. Ovarian cancer organoids fulfill this need, providing a controlled model that can respond to TCM treatments and offer insights into their complex therapeutic dynamics (Kopper et al., 2019; Maenhoudt et al., 2020). These organoids have surpassed traditional models by accurately simulating the tumor's microenvironment, including the preservation of genomic and histological tumor features, which is vital for personalized medicine (de Witte et al., 2020; Senkowski et al., 2023; Zhang et al., 2021). Our previously research has highlighted the organoids' ability to maintain a rich immune context and vasculature, crucial for studying the formula's impact on cisplatin sensitivity (Zhao et al., 2024). By avoiding enzymatic digestion and Matrigel, these organoids offer a more authentic *in vivo*-like model, making them ideal for exploring TCM's role in immunotherapy and serving as a bridge between traditional and modern treatment strategies.

In this study, we validated the therapeutic effects of the ZMYL formula on ovarian cancer organoids based on our network pharmacology predictions. The organoids demonstrated a dose-dependent response, exhibiting morphological changes and alterations in cellular architecture, particularly a reduction in size and structural sparsity at higher concentrations of the ZMYL formula. RNA sequencing analysis post-treatment revealed significant modulation of key pathways, highlighting the formula's ability to reshape the tumor's molecular landscape. Importantly, the treatment primarily targeted cell cycle signaling and immune response cells, indicating a focused immunomodulatory effect. These findings not only confirm our computational predictions but also emphasize the potential of the ZMYL formula to specifically influence critical immune cell populations, paving the way for enhanced immunotherapeutic strategies in ovarian cancer.

Materials and methods

Ovarian cancer tissue collection

Our study encompassed a total of 21 ovarian cancer tissue (Table 1) samples collected post-surgically from patients at the Obstetrics and Gynecology Hospital of Fudan University. All samples were handled with the utmost care to preserve their integrity for research purposes. This study was conducted in compliance with the ethical guidelines and received approval from the Ethics Committee of the Obstetrics and Gynecology Hospital of Fudan University (Approval Number: kyy2023-06; Approval Date: 2023.2.27). All patients provided written informed consent to participate in the study, and they were aware that the data would be published in accordance with ethical standards.

Table 1
The patients' information.

Patient number	Age	Diseases	Tumor location
OV023	72	High-grade serous carcinoma of the fallopian tube	NA
OV043	45	Ovarian clear cell carcinoma	NA
OV045	60	High-grade serous carcinoma of the fallopian tube and ovary	Peritoneum
OV049	55	High-grade serous carcinoma of the fallopian tube	Left ovary
OV054	60	High-grade serous carcinoma of the fallopian tube	Omentum
OV055	57	ovarian endometrioid carcinoma	Right ovary
OV063	70	High-grade serous carcinoma of the fallopian tube	NA
OV064	52	High-grade serous carcinoma of the fallopian tube	Left adnexa
OV069	71	High-grade serous carcinoma of the fallopian tube	Primary adnexal mass
OV075	55	High-grade serous carcinoma of the ovary	NA
OV076	59	High-grade serous carcinoma of the fallopian tube	Right tubal mass
OV077	65	High-grade serous carcinoma of the ovary	NA
OV078	67	High-grade serous carcinoma of the fallopian tube	NA
OV080	60	High-grade serous carcinoma of the fallopian tube	Left adnexal mass
OV081	50	High-grade serous carcinoma of the fallopian tube	NA
OV082	55	High-grade serous carcinoma of the fallopian tube	NA
OV083	46	High-grade serous carcinoma of the fallopian tube and ovary	Left and right adnexal masses
OV084	64	High-grade serous carcinoma of the fallopian tube and ovary	right adnexal mass
OV086	66	Ovarian clear cell carcinoma	Pelvis, right adnexa
OV087	69	High-grade serous carcinoma of the fallopian tube	Right adnexal mass
OV088	42	Ovarian clear cell carcinoma	Pelvis, right adnexa

Ovarian cancer organoids culture

Ovarian cancer tissues were collected and processed for organoid culture using organoid washing buffer (LSTO00100201; Shanghai LiSheng Biotech, China). Tissues were sheared into 3mm fragments and cultured in ovarian cancer culture medium (LSTO001004; Shanghai LiSheng Biotech, China) at 37°C and 5% CO2, with medium changes every seven days (Cao et al., 2023; Zhao et al., 2024). Organoids were passaged by harvesting with cell scrapers, centrifuging to remove supernatant, and fragmenting to 3mm before transfer to fresh medium. Successful culture was confirmed by the rounding of organoid edges, with growth monitored using an inverted microscope (DMi1, Leica, USA).

HE and IHC staining

Paraffin-embedded ovarian cancer tissue sections and ovarian cancer organoids sections were processed for both hematoxylin and eosin (H&E) staining and immunohistochemical (IHC) analysis. For H&E staining, sections were deparaffinized and stained with hematoxylin (WAS30011, Wasci) and eosin (WAS30012, Wasci) to visualize cellular structures, followed by dehydration, clearing, and mounting with neutral balsam (National Medicine 10004160). For IHC, after deparaffinization and antigen retrieval, the sections were incubated with

primary antibodies against Ki67 (MA5-14520, ThermoFisher) and PAX8 (10336-1-AP, Proteintech) at a dilution of 1:1000 overnight at 4°C. This was followed by incubation with a biotinylated secondary antibody and an avidin-biotin-peroxidase complex, with immune complexes visualized using a DAB substrate kit (ab64328, Abcam). The slides were then counterstained, dehydrated, and mounted for examination under a light microscope, enabling the assessment of cellular morphology and protein expression patterns within the ovarian cancer tissues.

Single cell RNA sequencing and annotation

Single-cell RNA sequencing was applied to two patient-derived tissue samples and three organoid samples to explore cellular heterogeneity. Utilizing a specific organoid dissociation kit from Shanghai LiSheng Biotech, individual cells were isolated, erythrocytes removed, and cell viability assessed with Solarbio lysis solution and a Countstar® Rigel S2 analyzer. Libraries for sequencing were prepared with the SeekOne® kit, followed by cDNA synthesis, purification, and amplification with unique molecular identifiers. The libraries were cleaned, quantified with KAPA Biosystems qPCR, and sequenced on the Illumina HiSeq 4000 platform. Data analysis with Cell Ranger and Seurat software elucidated the cellular landscape within the ovarian cancer samples and organoids. The expression matrix was generated using Cell Ranger v8.0.0 and SeekoulTools v1.2.1, depending on the type of single-cell sequencing kit used. Different samples were integrated using Canonical Correlation Analysis (CCA) in Seurat v5.1.0. The annotation was generated manually based on marker genes.

Preparation of ZMYL extracts and UHPLC/Q-TOF/MS

The ZMYL formula (provided by Longhua Hospital, Shanghai University of Traditional Chinese Medicine, China) contains ten species of herbal medicines (Table 2). The ten component species were identified by the Department of Pharmacy of Longhua Hospital. Add 10 times the amount of water and soak for 30 min. After boiling, simmer for 30 min. Strain the residue, add 8 times the amount of water to boil, simmer for half an hour. Strain, combine filtrate twice and concentrate under pressure to 850 ml. 2 ml of concentrated liquid was centrifuged in a centrifuge tube and centrifuged at 12,000 RPM for 5 min. The supernatant was obtained. Ultra-high-performance liquid chromatography-quadrupole time-of-flight mass spectrometry (UHPLC/Q-TOF/MS) was used to analyse the samples. Chromatographic separation was achieved on an Agilent SB C18 analytical HPLC column (2.1 × 150 mm, 1.8 μm).

ZMYL formula ingredients collection and target screening

The ZMYL formula, comprised of 10 TCM extracts, was evaluated for its component compounds' potential targets. Databases including TCMSP (Ru et al., 2014), HERB (Fang et al., 2021), TCM-ID (Chen et al., 2006), and BATMA-TCM (Liu et al., 2016) were searched to identify these targets. The selection of active compounds was based on oral bioavailability (OB) ≥30% and drug likeness (DL) ≥0.18. DrugBank (Knox et al., 2024) was then used to associate targets with these active compounds.

Table 2
The composition of ZMYL.

Pharmaceutical	Chinese name	Part used	Ratio
Radix Astragali	Huangqi	Root	15
Codonopsis pilosula	Dangshen	Root	15
Lycium barbarum	Gouqizi	Fruit	15
Scutellariae Barbatae	Banzhilian	Aerial part	18
Akebia trifoliata Koidz	Bayuezha	Fruit	18
Asparagus cochinchinensis	Tiandong	Root and Rhizome	12
Paeonia lactiflora pallas	Baishao	Root	15
Rhizoma Atractylodis Macrocephalae	Baizhu	Root and Rhizome	9
Aucklandia lappa Decne	Muxiang	Root	9
Rehmannia glutinosa Libosch	Shengdihuang	Root and Rhizome	12

Ovarian cancer-related targets collection and differential gene expression analysis

Ovarian cancer-related targets were identified from GeneCards (Stelzer et al., 2016), DisGeNET (Pinero et al., 2020), DrugBank (Knox et al., 2024), TTD (Wang et al., 2020), and OMIM (Amberger et al., 2015) using "ovarian cancer" as the search term. Visualization of the targets was facilitated by the R package UpSetR. The GEO database was also mined for DEGs from the GES26712 dataset, contrasting 10 normal samples with 185 ovarian cancer samples. DEGs were identified using the R Limma package with the criteria of $|\log2FC| > 1$ and Padjust < 0.05. Visualization of these DEGs was achieved using ggplot2 for volcanic maps and pheatmap for heatmaps.

Network construction, PPI network, and molecular docking

The intersection of targets associated with the ZMYL formula, ovarian cancer-related targets, and DEGs was determined using the R package VennDiagram (version 1.7.1). Networks illustrating the relationships among disease, drugs, compounds, targets, and biological processes were constructed in Cytoscape (version 3.8.2). The STRING database was utilized to build a PPI network for the key targets, applying a confidence threshold of 0.4 and hiding disconnected nodes. Molecular docking was performed to validate the interactions between active ingredients of the ZMYL formula and key targets. The three-dimensional (3D) structures of the selected targets were downloaded from the RSCB PDB (Burley et al., 2021). AutoDock Tools (version 1.5.6) was used to remove water molecules, isolate proteins, add nonpolar hydrogen, and calculate Gasteiger charges for the target structures, which were then saved in PDBQT format. The two-dimensional (2D) structures of the common active ingredients were downloaded from the PubChem (Kim et al., 2019). The 2D structure was processed and transformed into PDB format through Chem3D, and were saved in PDBQT format as docking ligand in AutoDock (version 1.5.6). The selected target proteins were used as receptors, and the active ingredient quercetin was used as ligand. The active site of the molecular docking was determined by the ligand coordinate in the target protein complex. AutoDock vina (version 1.1.2) was used for molecular docking simulation, setting energy <-5 kcal/mol as strong. A total of 20 conformations were generated for each docking result, and the conformation with the best affinity was chosen as the final docking conformation and was visualized using PyMol (version 2.4.1).

Functional detection of ZMYL formula in ovarian cancer organoids

In the investigation of ZMYL formula's impact on ovarian cancer organoids, the formula's lyophilized powder was dissolved in water and filtered, then applied to organoids at concentrations of 25 ng/mL, 2.5 μg/mL, 250 μg/mL, and 25 mg/mL. Organoids were observed and photographed at set time points to assess their response to treatment. For the OV081 organoids, histological assessment was performed on Day 14 post-treatment through paraffin embedding and section staining to examine cellular morphology. Meanwhile, RNA from OV087 and OV088 organoids was collected 48 h after treatment for subsequent transcriptomic analysis, aiming to explore the molecular effects of the ZMYL formula.

RNA-sequencing and analysis

For the RNA sequencing component of our study, organoids were collected and preserved in TRIzol Reagent (15596018, ThermoFisher,

USA) for RNA stabilization before being stored at -80°C. Total RNA was isolated using the RNA Easy Fast Tissue/Cell Kit (4992732, Tiangen, China), and RNA quality was assessed with a Qubit 3.0 Fluorometer (ThermoFisher, Waltham, England). Reverse transcription and library preparation were performed using the RT Kit (KR118, TIANGEN, China) and the RNA Library Prep Kit (E7530L, NEB, USA), respectively. Sequencing was conducted on an Illumina HiSeq 4000 platform, yielding data analyzed based on fragments per kilobase of transcript per million mapped reads (FPKM). Differential gene expression analysis was carried out using R and Morpheus online software, with functional and pathway enrichment analyses performed via the g:Profiler database.

Statistical analysis

Data, derived from a minimum of three replicates, are expressed as the mean ± standard deviation across separate experiments. Statistical evaluations were conducted utilizing GraphPad Prism version 8.

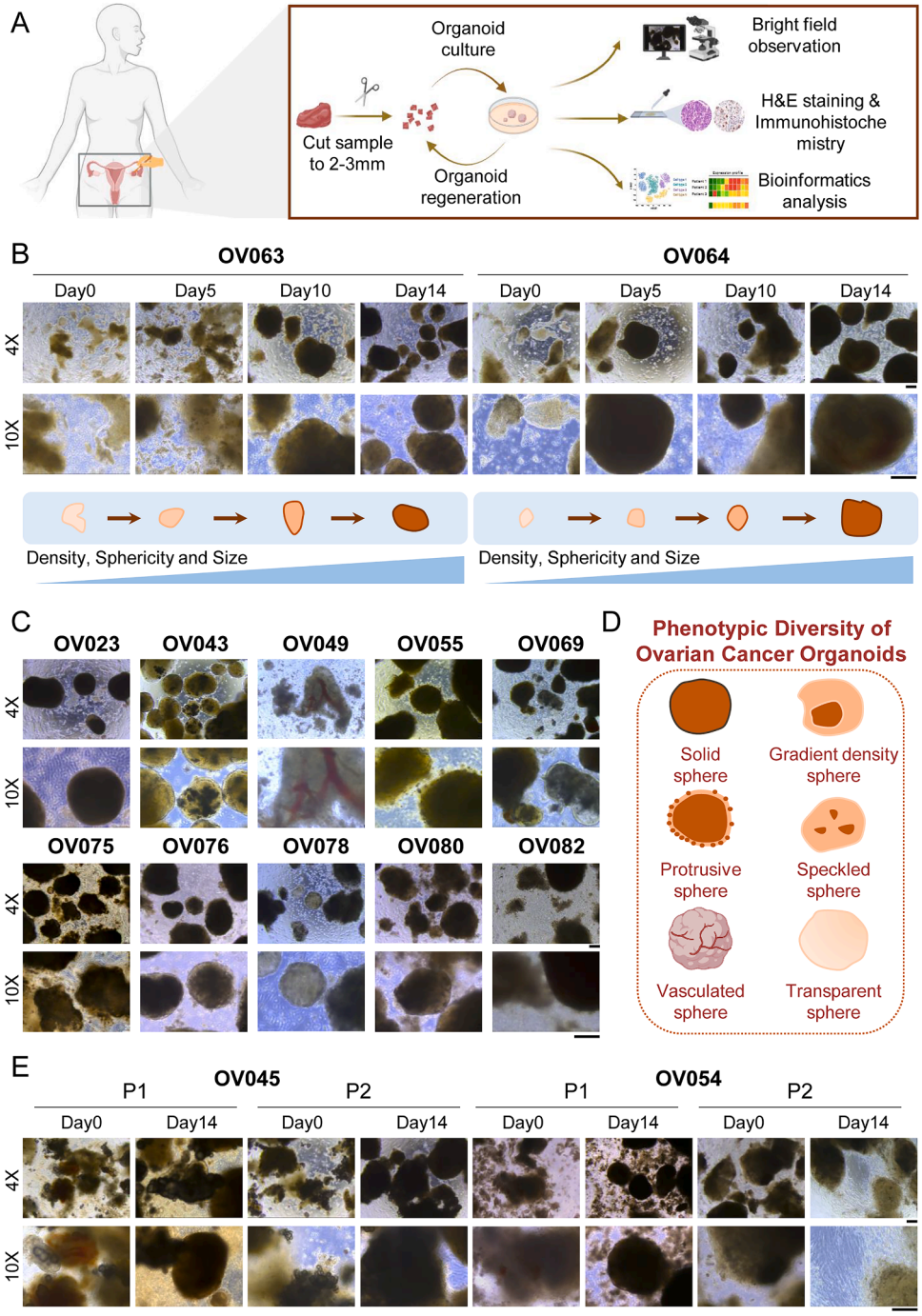

Fig. 1. Establishment of ovarian cancer organoids. (A) Workflow diagram outlining the process of establishing ovarian cancer organoids, from initiation to analysis. (B) Growth progression of OV063 and OV064 organoids captured by bright-field images at Days 0, 5, 10, and 14. Accompanying schematics indicate the increase in density, sphericity, and size over time. (C) Varied phenotypes of organoids from 10 distinct patient samples on Day 14, illustrating the phenotypic diversity. (D) Summary of organoid phenotypes, categorized as Solid, Gradient Density, Protrusive, Speckled, Vasculated, and Transparent. (E) Growth comparison of OV045 and OV054 organoids at Passage 0 (P0) and Passage 1 (P1), indicating their growth kinetics. Scale Bar: 200 μm.

Results

Establishment and morphological tracking of ovarian cancer organoids

To preserve the native microenvironment of ovarian tumor tissues and prevent clonal selection, we established ovarian cancer organoids without enzymatic dissociation or the use of Matrigel, as outlined in the workflow diagram (Fig. 1A). This approach facilitated the maintenance of tissue architecture and cellular interactions, critical for reflecting the *in vivo* tumor ecosystem. The organoids were cultured from mechanically sheared tissue fragments and monitored for growth and morphological changes using bright-field imaging, which captured the increase in density, sphericity, and size over time (Fig. 1B). On Day 14, the organoids exhibited a spectrum of phenotypes, underscoring the heterogeneity of ovarian cancer and the representativeness of our model system (Fig. 1C). Phenotypes were systematically categorized into six distinct groups, aiding in the comparative analysis of organoid characteristics (Fig. 1D). A growth kinetics comparison between passages demonstrated the adaptability and growth potential of these organoids, highlighting the importance of passaging in organoid culture (Fig. 1E). These results pave the way for our upcoming investigations into the organoids' internal structure and cellular makeup, which are expected to yield additional understanding of their biological characteristics and their value as research models for ovarian cancer.

Comprehensive characterization of ovarian cancer organoids and cellular heterogeneity

Our ovarian cancer organoid system, designed to closely mimic native tumor characteristics, was validated through comprehensive histological and cellular analyses. H&E staining (Fig. 2A) revealed well-preserved tissue architecture across organoids from six patients, while PAX8 staining confirmed their epithelial origin (Fig. 2B). Ki67 staining indicated active proliferation, demonstrating the organoids' viability (Fig. 2C).

The single-cell RNA sequencing analysis of ovarian cancer tissues and organoids has revealed a complex cellular landscape that mirrors the heterogeneity of the original tumors, with a high degree of overlap in cellular distributions observed between organoids and their corresponding tissues (Fig. 3A, B). This suggests that the organoid system can replicate a broad range of cell types and proportions, preserving the sample-specific heterogeneity. The annotated cluster map categorizes the cells into thirteen distinct groups, including various immune cells such as B cells, marcrophages, proliferating T cells and other T cells, indicating the organoid culture system's potential for studying immune-related therapies and drug responses (Fig. 3C). The marker genes for each cluster, displayed in (Fig. 3D), further highlight the molecular diversity of the cell types present. A detailed analysis of different types of T cells, as shown in (Fig. 3E, F), reveals the expression patterns of genes associated with distinct T cell states, including activation, exhaustion, and cytotoxicity, providing crucial insights into the impact of TCM

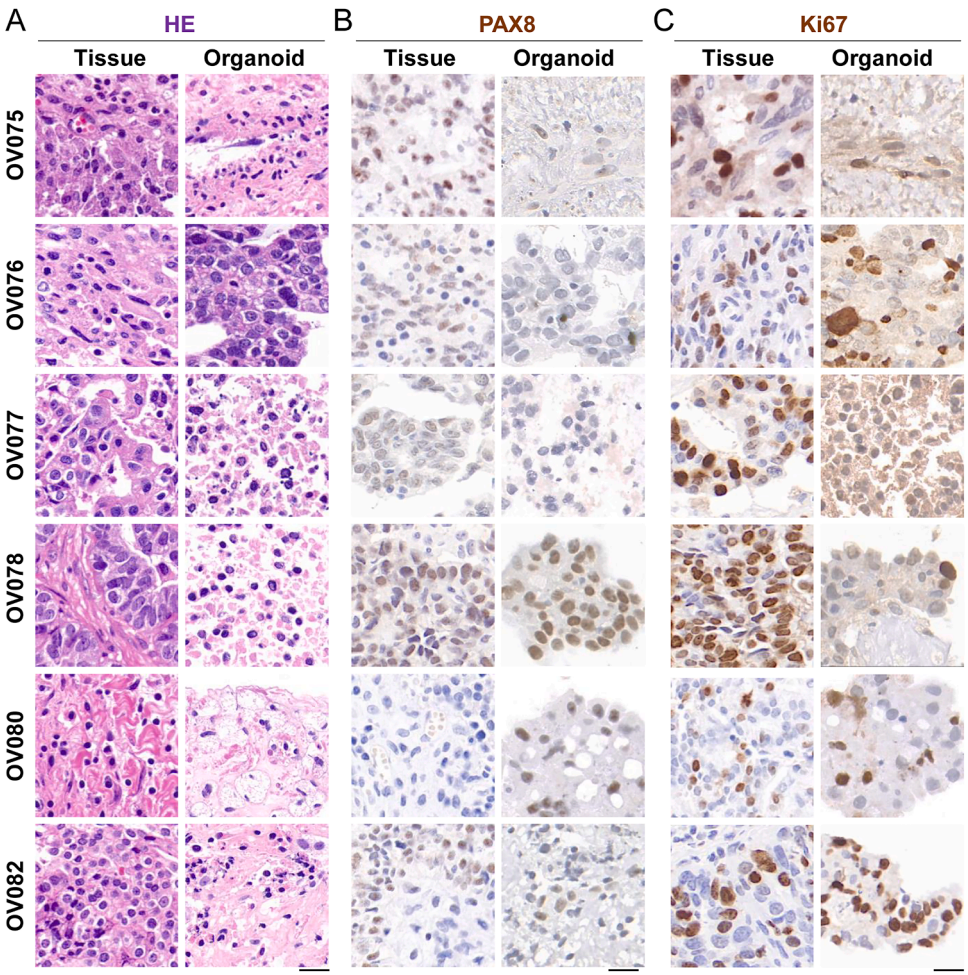

Fig. 2. Ovarian cancer organoid characterization. (A) H&E staining of organoids from six patients (OV075, OV076, OV077, OV078, OV080, and OV082), showcasing cellular arrangement and tissue structure. (B) PAX8 staining confirms the organoids' ovarian epithelial origin. (C) Ki67 staining assesses the organoids' proliferative activity. Scale Bar: 20 μm.

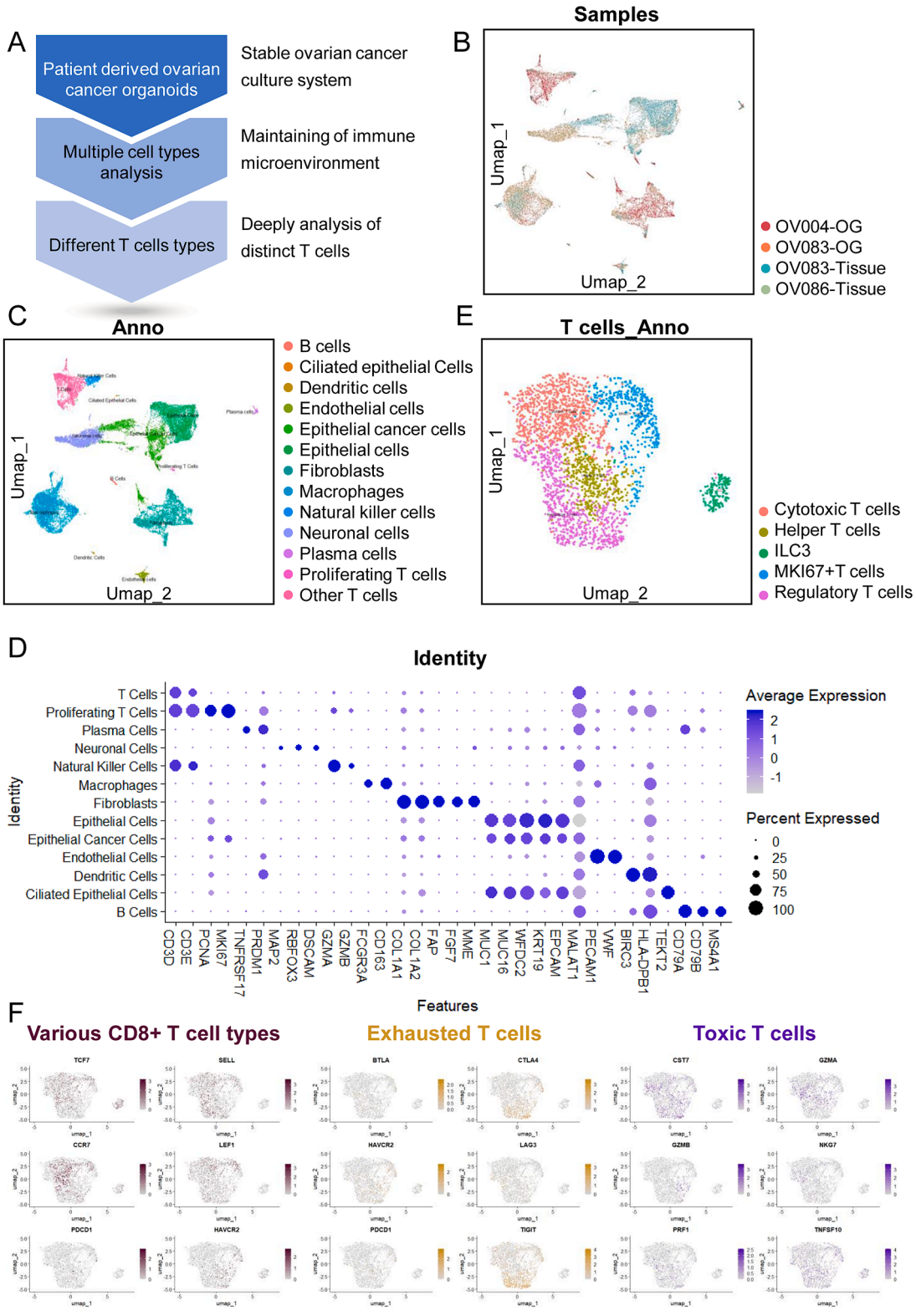

Fig. 3. Single-cell RNA sequencing of ovarian cancer tissues and organoids. (A) The overview of the single-cell RNA sequencing approach. (B) Distribution plots of ovarian cancer tissues (OV083, OV086) and organoids (OV004, OV0083) reveal the cellular heterogeneity within the samples. (C) The annotated cluster map delineates thirteen distinct cell populations, including B cells, ciliated epithelial cells, dendritic cells, endothelial cells, epithelial cancer cells, epithelial cells, fibroblasts, macrophages, natural killer cells, neuronal cells, plasma cells, proliferating T cells and other T cells, providing a comprehensive view of the cellular composition. (D) The marker genes characteristic of each cell cluster, providing a molecular overview. (E) The annotated cluster map delineates five different types of T cells, including cytotoxic T cells, helper T cells, ILC3, MKI67+ T cells and regulatory T cells. (F) Subgroup analysis of CD8-positive T cells, differentiated by gene expression profiles, distinguishes among various T cell states, including activated, exhausted, and toxic phenotypes.

treatments like the ZMYL formula on the tumor's immune microenvironment. These results underscore the organoid model's potential in advancing research into immunotherapeutic strategies for ovarian cancer.

Network pharmacology-driven identification of ZMYL formula's therapeutic targets and pathways in ovarian cancer

Following the establishment of an organoid system that recapitulates the immune microenvironment of ovarian cancer, we delved into the therapeutic effects and underlying mechanisms of the Zengmian Yiliu (ZMYL) formula (Figs. 4 and 5A) using a network pharmacology approach. This analysis was crucial for identifying the active constituents and pathways that the ZMYL formula might target in ovarian cancer. Our analysis began with the identification of formula targets from OMIM (Amberger et al., 2015), TCMSP (Ru et al., 2014), HERB (Fang et al., 2021), TCM-ID (Ru et al., 2014) and BATMAN-TCM (Liu et al., 2016) (Table 3), and the collection of ovarian cancer therapeutic targets from GeneCards (Stelzer et al., 2016), DisGeNET (Pinero et al., 2020) and DrugBank (Knox et al., 2024) (Fig. 5B). We further examined the genomic data using the GES26712 dataset, revealing a total of 1768 DEGs in ovarian cancer, with distinct upregulation and downregulation patterns visualized in a volcanic map (Fig. 5C). Consolidating the overlapping targets from the formula, ovarian cancer, and DEGs, we pinpointed a core set of 34 targets that may be modulated by the ZMYL formula (Fig. 5D). A subsequent disease-drug-compound-target network construction revealed 18 bioactive compounds from eight herbs that potentially interact with these genes, forming a network with 221 edges indicative of the formula's therapeutic pathways (Fig. 5E). To elucidate the molecular interactions within this network, a PPI network was constructed, highlighting key regulatory genes that the ZMYL formula may target, as reflected by the nodes' size and darkness (Fig. 5F). Lastly, molecular docking analysis provided insights into the specific interactions between the formula's active ingredients, such as diosgenin, baicalein, and quercetin, with key targets like TP53, JUN, VEGFA, ERBB2, MMP2 and CAV1, as shown in the molecular docking patterns

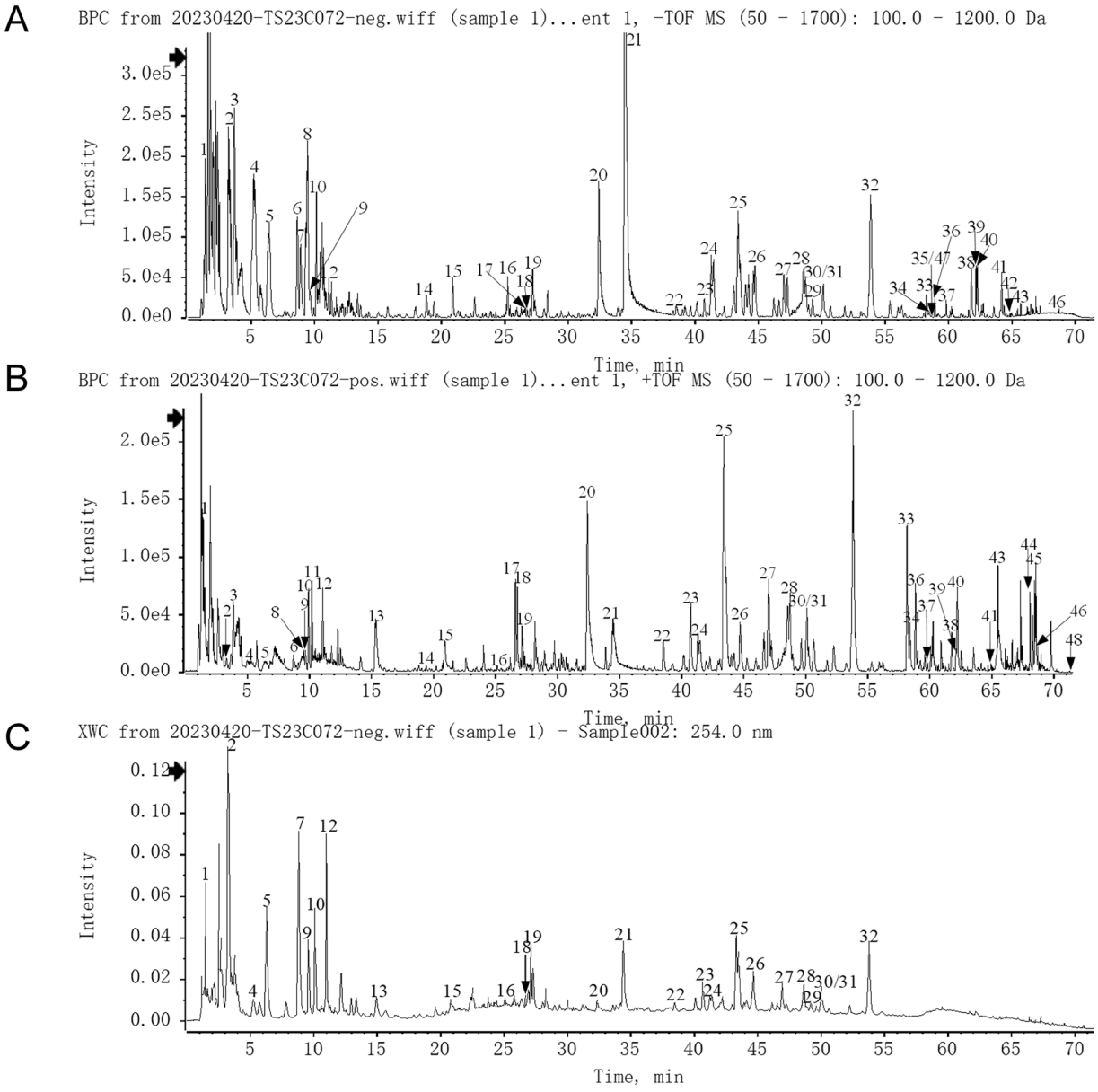

Fig. 4. UPLC-QTOF-MS analysis of ZMYL formula ingredients. (A) Representative ion chromatogram of ZMYL Formula in the negative mode. (B) Representative ion chromatogram of ZMYL Formula in the positive mode. (C) UPLC UV chromatogram of ZMYL compound sample -UV 254 nm.

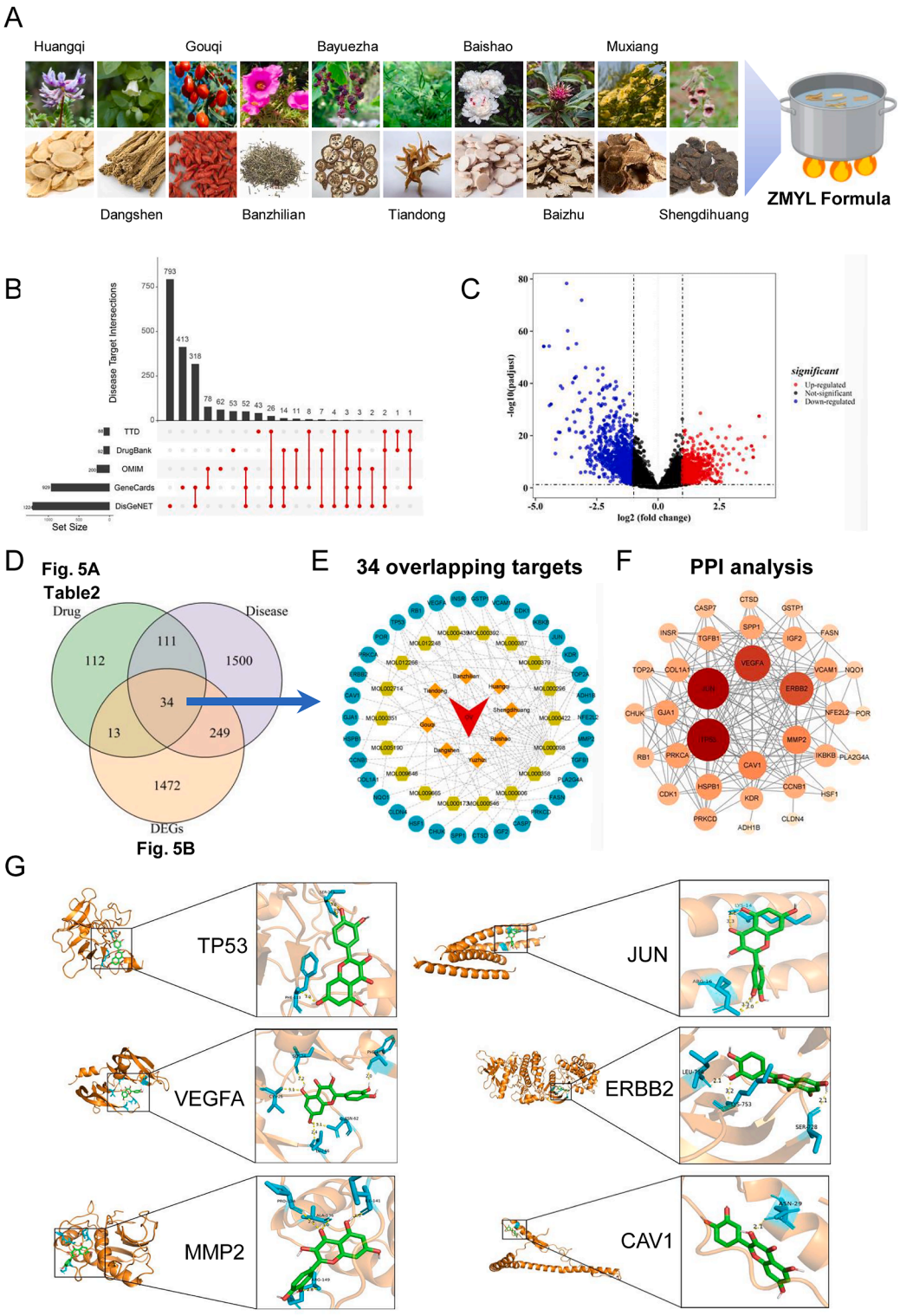

Fig. 5. Disease-drug-compound-target network construction of ZMYL formula. (A) Nature medical plants and traditional Chinese medicine for ZMYL formula. (B) The network construction begins with the identification of ovarian cancer targets from five databases: GeneCards, DisGeNET, DrugBank, TTD, and OMIM. A comparative bar chart details the number of unique and shared targets from each database, with a visual dot representation indicating the intersection of these datasets. (C) A volcanic map illustrates the differential gene expression in ovarian cancer, with red dots for up-regulated genes, blue for down-regulated, and black for non-significant genes, offering a snapshot of the genetic alterations associated with the disease. (D) The identification of overlapping targets between ovarian cancer and the ZMYL formula, along with DEGs, reveals 34 common candidate genes that may be key to the formula's therapeutic effects. (E) The Disease-Drug-Compound-Target network visually maps the interactions between 8 herbs and 18 bioactive compounds from the ZMYL formula and the 34 overlapping genes, highlighting 221 edges that represent potential therapeutic pathways. (F) The PPI network of these overlapping genes emphasizes the importance of specific genes in the treatment of ovarian cancer, with node size and darkness reflecting gene significance in the disease's molecular mechanisms. (G) Molecular docking patterns demonstrate the specific interactions between active ingredients like diosgenin, baicalein, and quercetin with key targets such as TP53, JUN, VEGFA, ERBB2, MMP2, and CAV1, suggesting the potential molecular mechanisms of the ZMYL formula's therapeutic action in ovarian cancer treatment.

Table 3
The compounds in ZMYL satisfying OB≥30% and DL≥0.18.

Molecule ID	Molecule name	OB %	DL	Herb name
MOL000211	Mairin	55.38	0.78	Huangqi/Muxiang/Baishao
MOL000239	Jaranol	50.83	0.29	Huangqi
MOL000296	hederagenin	36.9	0.75	Huangqi
MOL000033	(3S,8S,9S,10R,13R,14S,17R)-10,13-dimethyl-17-[(2R,5S)-5-propan-2-yloctan-2-yl]-2,3,4,7,8,9,11,12,14,15,16,17-dodecahydro-1H-cyclopenta[a]phenanthren-3-ol	36.23	0.78	Huangqi/Baizhu
MOL000354	isorhamnetin	49.6	0.31	Huangqi
MOL000371	3,9-di-O-methylnissolin	53.74	0.48	Huangqi
MOL000374	5′-hydroxyiso-muronulatol-2′,5′-di-O-glucoside	41.72	0.69	Huangqi
MOL000378	7-O-methylisomucronulatol	74.67	0.30	Huangqi
MOL000379	9,10-dimethoxypterocarpan-3-O-β-D-glucoside	36.74	0.92	Huangqi
MOL000380	(6aR,11aR)-9,10-dimethoxy-6a,11a-dihydro-6H-benzofurano[3,2-c]chromen-3-ol	64.26	0.42	Huangqi
MOL000387	Bifendate	31.10	0.67	Huangqi
MOL000392	formononetin	69.67	0.21	Huangqi
MOL000398	isoflavanone	109.99	0.30	Huangqi
MOL000417	Calycosin	47.75	0.24	Huangqi
MOL000422	kaempferol	41.88	0.24	Huangqi/Baishao
MOL000433	FA	68.96	0.71	Huangqi
MOL000438	(3R)-3-(2-hydroxy-3,4-dimethoxyphenyl)chroman-7-ol	67.67	0.26	Huangqi
MOL000439	isomucronulatol-7,2′-di-O-glucosiole	49.28	0.62	Huangqi
MOL000442	1,7-Dihydroxy-3,9-dimethoxy pterocarpene	39.05	0.48	Huangqi
MOL000098	quercetin	46.43	0.28	Huangqi/Banzhilian/Tiandong/Gouqi
MOL001006	poriferasta-7,22E-dien-3beta-ol	42.98	0.76	Dangshen
MOL002140	Perlolyrine	65.95	0.27	Dangshen
MOL002879	Diop	43.59	0.39	Dangshen
MOL003036	ZINC03978781	43.83	0.76	Dangshen
MOL000449	Stigmasterol	43.83	0.76	Dangshen/Banzhilian/Tiandong/Gouqi/Muxiang
MOL003896	7-Methoxy-2-methyl isoflavone	42.56	0.20	Dangshen/Tiandong
MOL004355	Spinasterol	42.98	0.76	Dangshen
MOL004492	Chrysanthemaxanthin	38.72	0.58	Dangshen
MOL005321	Frutinone A	65.90	0.34	Dangshen
MOL000006	luteolin	36.16	0.25	Dangshen/Banzhilian
MOL006554	Taraxerol	38.40	0.77	Dangshen
MOL006774	stigmast-7-enol	37.42	0.75	Dangshen
MOL007059	3-beta-Hydroxymethyllenetanshiquinone	32.16	0.41	Dangshen
MOL007514	methyl icosa-11,14-dienoate	39.67	0.23	Dangshen
MOL008391	5alpha-Stigmastan-3,6-dione	33.12	0.79	Dangshen
MOL008393	7-(beta-Xylosyl)cephalomannine_qt	38.33	0.29	Dangshen
MOL008397	Daturilin	50.37	0.77	Dangshen
MOL008400	glycitein	50.48	0.24	Dangshen/Gouqi
MOL008406	Spinoside A	39.97	0.40	Dangshen
MOL008407	(8S,9S,10R,13R,14S,17R)-17-[(E,2R,5S)-5-ethyl-6-methylhept-3-en-2-yl]-10,13-dimethyl-1,2,4,7,8,9,11,12,14,15,16,17-dodecahydrocyclopenta[a]phenanthren-3-one	45.40	0.76	Dangshen
MOL008411	11-Hydroxyrankinidine	40.00	0.66	Dangshen
MOL001040	(2R)-5,7-dihydroxy-2-(4-hydroxyphenyl)chroman-4-one	42.36	0.21	Banzhilian
MOL012245	5,7,4′-trihydroxy-6-methoxyflavanone	36.63	0.27	Banzhilian
MOL012246	5,7,4′-trihydroxy-8-methoxyflavanone	74.24	0.26	Banzhilian
MOL012248	5-hydroxy-7,8-dimethoxy-2-(4-methoxyphenyl)chromone	65.82	0.33	Banzhilian
MOL012250	7-hydroxy-5,8-dimethoxy-2-phenyl-chromone	43.72	0.25	Banzhilian
MOL012251	Chrysin-5-methylether	37.27	0.20	Banzhilian
MOL012252	9,19-cyclolanost-24-en-3-ol	38.69	0.78	Banzhilian
MOL002776	Baicalin	40.12	0.75	Banzhilian
MOL012254	campesterol	37.58	0.71	Banzhilian/Shengdihuang
MOL000953	CLR	37.87	0.68	Banzhilian/Gouqi
MOL000358	beta-sitosterol	36.91	0.75	Banzhilian/Tiandong/Gouqi/Yuzhizi/Baishao/Shengdihuang
MOL012266	rivularin	37.94	0.3663	Banzhilian
MOL001973	Sitosteryl acetate	40.39	0.85	Banzhilian
MOL012269	Stigmasta-5,22-dien-3-ol-acetate	46.44	0.86	Banzhilian
MOL012270	Stigmastan-3,5,22-triene	45.03	0.71	Banzhilian
MOL000173	wogonin	30.68	0.23	Banzhilian
MOL001735	Dinatin	30.97	0.27	Banzhilian
MOL001755	24-Ethylcholest-4-en-3-one	36.08	0.76	Banzhilian
MOL002714	baicalein	33.52	0.21	Banzhilian
MOL002719	6-Hydroxynaringenin	33.23	0.24	Banzhilian
MOL002915	Salvigenin	49.07	0.33	Banzhilian
MOL000351	Rhamnazin	47.14	0.34	Banzhilian
MOL000359	sitosterol	36.91	0.75	Banzhilian/Tiandong/Yuzhizi/Muxiang/Baishao
MOL005190	eriodictyol	71.79	0.24	Banzhilian
MOL005869	daucostero_qt	36.91	0.75	Banzhilian
MOL008206	Moslosooflavone	44.09	0.25	Banzhilian

(*continued on next page*)

Table 3 (*continued*)

Molecule ID	Molecule name	OB %	DL	Herb name
MOL000020	12-senecioyl-2E,8E,10E-atractylentriol	62.40	0.22	Baizhu
MOL000021	14-acetyl-12-senecioyl-2E,8E,10E-atractylentriol	60.31	0.31	Baizhu
MOL000022	14-acetyl-12-senecioyl-2E,8Z,10E-atractylentriol	63.37	0.30	Baizhu
MOL000028	α-Amyrin	39.51	0.76	Baizhu
MOL000049	3β-acetoxyatractylone	54.07	0.22	Baizhu
MOL000072	8β-ethoxy atractylenolide III	35.95	0.21	Baizhu
MOL003889	methylprotodioscin_qt	35.12	0.86	Tiandong
MOL003891	pseudoprotodioscin_qt	37.93	0.87	Tiandong
MOL003901	Asparaside A_qt	30.60	0.86	Tiandong
MOL000546	diosgenin	80.88	0.81	Tiandong
MOL001323	Sitosterol alpha1	43.28	0.78	Gouqi
MOL003578	Cycloartenol	38.69	0.78	Gouqi
MOL001494	Mandenol	41.99	0.19	Gouqi
MOL001495	Ethyl linolenate	46.10	0.20	Gouqi
MOL001979	LAN	42.12	0.75	Gouqi
MOL005406	atropine	45.97	0.19	Gouqi
MOL005438	campesterol	37.58	0.71	Gouqi
MOL006209	cyanin	47.42	0.76	Gouqi
MOL007449	24-methylidenelophenol	44.19	0.75	Gouqi
MOL008173	daucosterol_qt	36.91	0.75	Gouqi
MOL010234	delta-Carotene	31.80	0.55	Gouqi
MOL009604	14b-pregnane	34.78	0.34	Gouqi
MOL009612	(24R)-4alpha-Methyl-24-ethylcholesta-7,25-dien-3beta-ylacetate	46.36	0.8398	Gouqi
MOL009615	24-Methylenecycloartan-3beta,21-diol	37.32	0.8	Gouqi
MOL009617	24-ethylcholest-22-enol	37.09	0.75	Gouqi
MOL009618	24-ethylcholesta-5,22-dienol	43.83	0.76	Gouqi
MOL009620	24-methyl-31-norlanost-9(11)-enol	38.00	0.75	Gouqi
MOL009621	24-methylenelanost-8-enol	42.37	0.77	Gouqi
MOL009622	Fucosterol	43.78	0.76	Gouqi
MOL009631	31-Norcyclolaudenol	38.68	0.81	Gouqi
MOL009633	31-norlanost-9(11)-enol	38.35	0.72	Gouqi
MOL009634	31-norlanosterol	42.20	0.73	Gouqi
MOL009635	4,24-methyllophenol	37.83	0.75	Gouqi
MOL009639	Lophenol	38.13	0.71	Gouqi
MOL009640	4alpha,14alpha,24-trimethylcholesta-8,24-dienol	38.91	0.76	Gouqi
MOL009641	4alpha,24-dimethylcholesta-7,24-dienol	42.65	0.75	Gouqi
MOL009642	4alpha-methyl-24-ethylcholesta-7,24-dienol	42.30	0.78	Gouqi
MOL009644	6-Fluoroindole-7-Dehydrocholesterol	43.73	0.72	Gouqi
MOL009646	7-O-Methylluteolin-6-C-beta-glucoside_qt	40.77	0.30	Gouqi
MOL009650	Atropine	42.16	0.19	Gouqi
MOL009651	Cryptoxanthin monoepoxide	46.95	0.56	Gouqi
MOL009653	Cycloeucalenol	39.73	0.79	Gouqi
MOL009656	(E,E)-1-ethyl octadeca-3,13-dienoate	42.00	0.19	Gouqi
MOL009660	methyl (1R,4aS,7R,7aS)-4a,7-dihydroxy-7-methyl-1-[(2S,3R,4S,5S,6R)-3,4,5-trihydroxy-6-(hydroxymethyl)oxan-2-yl]oxy-1,5,6,7a-tetrahydrocyclopenta[d]pyran-4-carboxylate	39.43	0.47	Gouqi
MOL009662	Lantadene A	38.68	0.57	Gouqi
MOL009664	Physalin A	91.71	0.27	Gouqi
MOL009665	Physcion-8-O-beta-D-gentiobioside	43.90	0.62	Gouqi
MOL009677	lanost-8-en-3beta-ol	34.23	0.74	Gouqi
MOL009678	lanost-8-enol	34.23	0.74	Gouqi
MOL009681	Obtusifoliol	42.55	0.76	Gouqi
MOL010929	glyceryl linolenate	38.14	0.31	Yuzhizi
MOL002882	[(2R)-2,3-dihydroxypropyl] (Z)-octadec-9-enoate	34.13	0.30	Yuzhizi
MOL008121	2-Monoolein	34.23	0.29	Yuzhizi
MOL008218	1-Monoolein	34.13	0.30	Yuzhizi
MOL010813	Benzo[a]carbazole	35.22	0.22	Muxiang
MOL010828	cynaropicrin	67.50	0.38	Muxiang
MOL010839	lappadilactone	38.56	0.73	Muxiang
MOL001910	11alpha,12alpha-epoxy-3beta-23-dihydroxy-30-norolean-20-en-28,12beta-olide	64.77	0.38	Baishao
MOL001918	paeoniflorgenone	87.59	0.37	Baishao
MOL001919	(3S,5R,8R,9R,10S,14S)-3,17-dihydroxy-4,4,8,10,14-pentamethyl-2,3,5,6,7,9-hexahydro-1H-cyclopenta[a]phenanthrene-15,16-dione	43.56	0.53	Baishao
MOL001921	Lactiflorin	49.12	0.80	Baishao
MOL001924	paeoniflorin	53.87	0.79	Baishao
MOL001925	paeoniflorin_qt	68.18	0.40	Baishao
MOL001928	albiflorin_qt	66.64	0.33	Baishao
MOL001930	benzoyl paeoniflorin	31.27	0.75	Baishao
MOL000492	(+)-catechin	54.83	0.24	Baishao

(Fig. 5G). In essence, our network pharmacology analysis has succinctly outlined the ZMYL formula's multi-targeted therapeutic strategy in ovarian cancer, laying the groundwork for subsequent organoid-based experiments and pharmacological inquiries.

Dose-dependent effects of ZMYL formula on ovarian cancer organoids

As a result of our network pharmacology predictions on the potential effects of the ZMYL formula in ovarian cancer, we sought to verify its therapeutic efficacy using a human ovarian organoids culture system

which has been proven to be a reliable platform for drug screening in ovarian cancer research (Cao et al., 2023; Zhao et al., 2024). The ZMYL formula's dose-dependent impact on ovarian cancer organoids is evident from the treatment efficacy flowchart (Fig. 6A), detailing the exposure of organoids from various patients to a gradient of formula concentrations. By Day 8, morphological changes were apparent, with (Fig. 6B) showing a reduction in size and shape alteration in organoids treated with higher concentrations. H&E staining by Day 14, as depicted in (Fig. 6C), revealed that escalating dosages of the ZMYL formula corresponded to a decrease in cellular density and an increase in structural

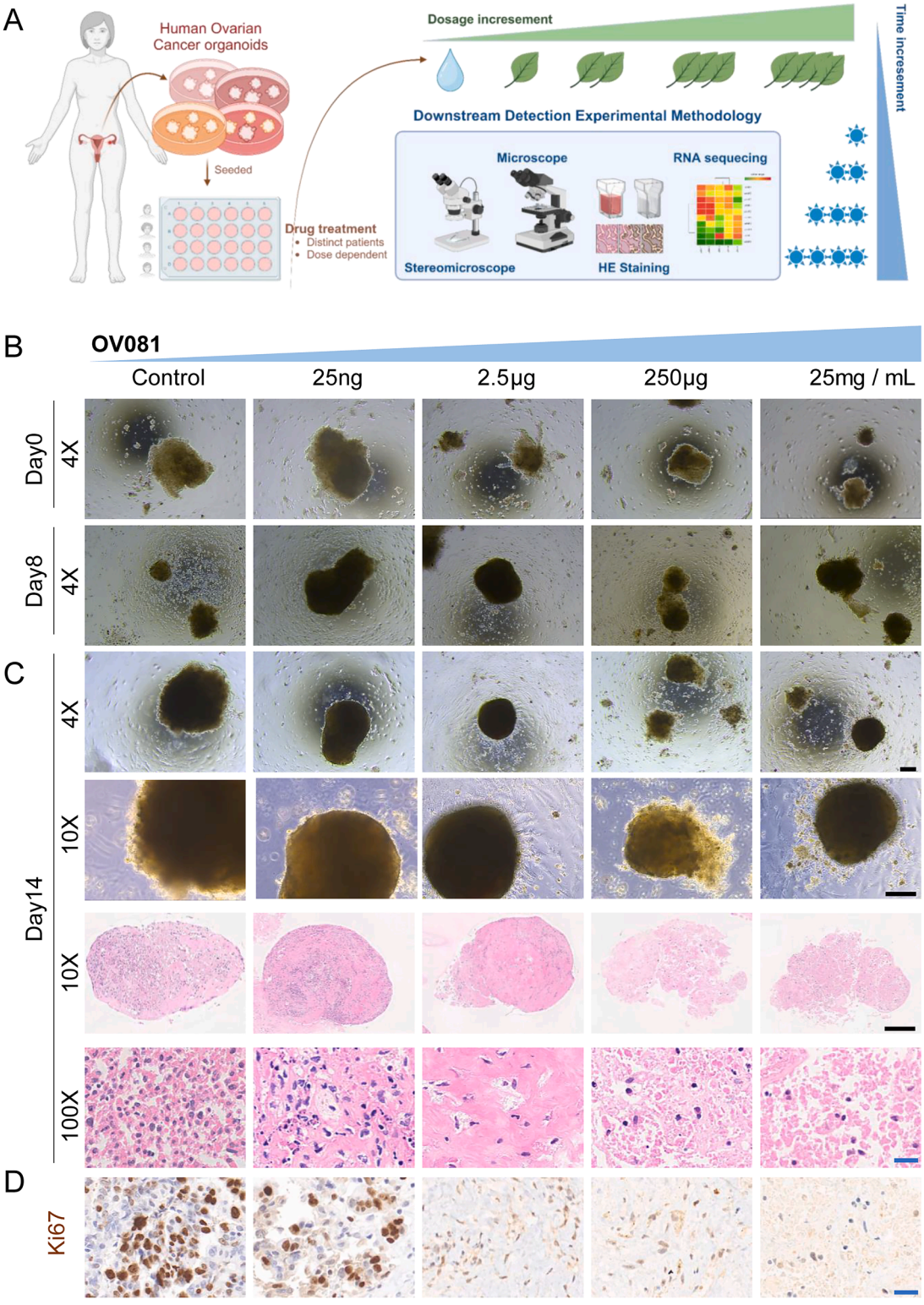

Fig. 6. Dose-dependent effects of ZMYL formula on ovarian cancer organoids. (A) Flowchart of the efficacy testing process of the ZMYL formula on organoids derived from different ovarian cancer patients. (B) Morphological comparison of organoids at Day 0 and Day 8 post-treatment with the ZMYL formula at various concentrations. (C) Day 14 organoid state and corresponding HE-stained sections, showcasing the dose-dependent effects on growth and morphology. (D) Ki67 immunohistochemical staining of organoids treated with different concentrations of ZMYL formula. Black scales: 200; Blue scale: 20 μm.

sparsity within the organoids. Furthermore, Ki67 immunohistochemical staining (Fig. 6D) demonstrated a significant reduction in Ki67-positive cells with increasing concentrations of ZMYL, indicating a decrease in cell proliferation. These findings indicate that the formula influences not only the growth but also the internal cellular architecture of ovarian cancer organoids, thereby substantiating its therapeutic potential as suggested by our initial computational analysis.

Modulation of cellular pathways by the ZMYL formula in ovarian cancer organoids

The time-lapse imaging of OV087 and OV088 organoids exposed to various concentrations of the ZMYL formula has captured the morphological changes over the course of 31 days, demonstrating the formula's impact on organoid growth and structure (Fig. 7A). The PCA analysis (Fig. 7B) reveals the transcriptional variance among the organoids, underscoring the diversity in their responses to the treatment. For the transcriptomic analysis, we used four different doses of ZMYL formula: 25 ng/mL, 2.5 μg/mL, 250 μg/mL, and 25 mg/mL. These doses were selected based on preliminary experiments to capture a range of pharmacological effects without complete cytotoxicity. The samples for RNA-seq were labeled as -1 (Control group), -3, -5, -7, and -9 (ZMYL treatment groups). The combined hierarchical clustering analysis (Fig. 7C) not only highlights the heterogeneity between patient samples but also distinguishes the treated groups from the controls, suggesting a clear effect of the ZMYL formula on gene expression patterns. Furthermore, the heatmaps correspond with the single-cell sequencing analysis, showcase the expression of T cell-related genes and the 34 target genes identified through network pharmacology (Fig. 7D, E). The significant binding interactions of six genes (*TP53, JUN, VEGFA, ERBB2, MMP2, CAV1*) marked with red arrows indicate their potential roles in mediating the formula's effects.

Trend analysis of OV087 and OV088 after ZMYL treatment revealed gene expression changes. In OV087, 5554 genes were downregulated and 1023 upregulated; in OV088, 4177 downregulated and 651 upregulated. Venn diagram analysis identified common genes affected in both organoids. This analysis pinpointed 853 downregulated and 68 upregulated genes in response to the ZMYL formula (Fig. 8A). The Gene Ontology (GO) analysis indicates that the formula's treatment leads to the suppression of cell cycle pathways and the activation of immune response pathways (Fig. 8B, C). Specifically, cell cycle-related genes such as *CCNB2, CDC20, CDC25A*, and *CDK10* are significantly downregulated, consistent with the reduced Ki67 staining observed in Fig. 6D. Additionally, immune-related genes like *CXCL10* are upregulated, suggesting the formula's potential to modulate the tumor's immune microenvironment. The heatmaps visually represent the expression changes of these cell cycle and immune response genes in OV087 and OV088 organoids (Fig. 8D, E), reinforcing the formula's potential to inhibit cancer cell proliferation while enhancing immune cell activity.

Discussion

Our study presents a cutting-edge approach to establishing ovarian cancer organoids, which is critical for advancing research in cancer therapeutics. By utilizing a method that avoids enzymatic dissociation and Matrigel, we have successfully maintained the native microenvironment of ovarian tumor tissues, as outlined in our methodology. This method, consistent with the sophisticated approaches reported in the literature, ensures the maintenance of diverse cellular components and their interactions, closely mirroring the complexity of the tumor's native environment (Kopper et al., 2019). The retention of patient-specific heterogeneity in our organoids is a significant advantage, as it ensures the potential for personalized medicine, a key aspect of modern cancer treatment strategies.

Network pharmacology is a powerful tool for understanding the complex mechanisms of multi-component therapies like the ZMYL formula. Our analysis identified 34 target genes, some significantly changed in RNA-seq data, confirming the reliability of network pharmacology in predicting therapeutic targets for TCM formulas. For instance, *CCNB1* and *CDK1* are well-known regulators of the cell cycle, and their dysregulation is linked to ovarian cancer progression (Kim et al., 2024; Yang et al., 2022). ZMYL's potential effect on these genes could be a mechanism through which it influences cell cycle arrest. Additionally, genes such as *VCAM1* is involved in immune cell recruitment and the formation of new blood vessels, respectively. *VCAM1* plays a crucial role in the adhesion and migration of immune cells to the tumor site (Samaha et al., 2018), while VEGFA is known for its role in angiogenesis and immune evasion. The impact of ZMYL on these genes might further explain its therapeutic effects on ovarian cancer. However, the six key targets from molecular docking (TP53, VEGFA, MMP2, JUN, ERBB2, and CAV1) showed no significant changes in RNA-seq. These genes might still influence the formula's effects through their downstream pathways, such as cell cycle regulation for TP53 (Qiu et al., 2022) and immune modulation for VEGFA (Wen et al., 2024). While molecular docking offers insights into drug-target interactions, further experimental validation is needed. Our study provides a foundation for understanding ZMYL's mechanisms, but more *in vitro* and *in vivo* experiments are required to fully explore its effects on these pathways. Compared to previous studies, our work innovatively combines network pharmacology with transcriptomic data to explore the multi-target effects of ZMYL on ovarian cancer. This integrative approach not only confirms known targets but also identifies novel potential targets, offering a more comprehensive understanding of the formula's therapeutic mechanisms. Our study offers fresh perspectives on TCM formula research in cancer treatment through two key innovations. First, we systematically investigated ZMYL's dual effects on cell cycle regulation and immune response modulation. Second, we used organoid models, the most realistic *in vitro* systems reflecting *in vivo* conditions, to observe TCM formulas' effects on cancer cell cycle and immune response. This approach enhances our understanding of TCM's role in cancer treatment.

The phenotypic responses of organoids to drug treatments can vary widely, as observed in our study and previously reported outcomes. While some organoids may exhibit shrinkage and edge disintegration (Zhao et al., 2024), others might show a reduction in migrating cells post-treatment (Cao et al., 2023). Interestingly, organoids treated with the ZMYL formula did not display drastic morphological changes but did exhibit internal structural disarray. This highlights the need for a multifaceted approach in assessing drug responses in organoids, including both morphological and molecular analyses.

Further, our study's gene expression analysis post-ZMYL formula treatment has provided valuable insights into the molecular changes within ovarian cancer organoids. The cell cycle-related genes *CCNB2, CDC20, CDC25A, CDK10*, and others, which we identified as being modulated by the ZMYL formula, are consistent with key regulators of cell division (Fig. 9). Notably, *CCNB2* has been reported to be involved in the G2/M transition of the cell cycle and is associated with poor prognosis in ovarian cancer (Ke et al., 2022). Similarly, *CDC20* and *CDC25A* are known to play crucial roles in cell cycle regulation and have been implicated in chemoresistance in ovarian cancer (Sun et al., 2021; Sun et al., 2019). The modulation of these genes by the ZMYL formula suggests a potential mechanism for its therapeutic effects. Immune-related genes such as *ABI3, ARHGDIB, CD1A*, and *CXCL10*, which were also found to be affected by the ZMYL formula, are known to play significant roles in immune cell function and tumor immunology. For instance, *CXCL10* is a chemokine that attracts immune cells to the tumor site and has been associated with improved survival in ovarian cancer patients (Bronger et al., 2016). The ability of the ZMYL formula to regulate these genes indicates its potential to modulate the tumor's immune microenvironment, which is a critical aspect of cancer immunotherapy. The differential gene expression we observed aligns with previous reports on the effects of traditional Chinese medicine in cancer

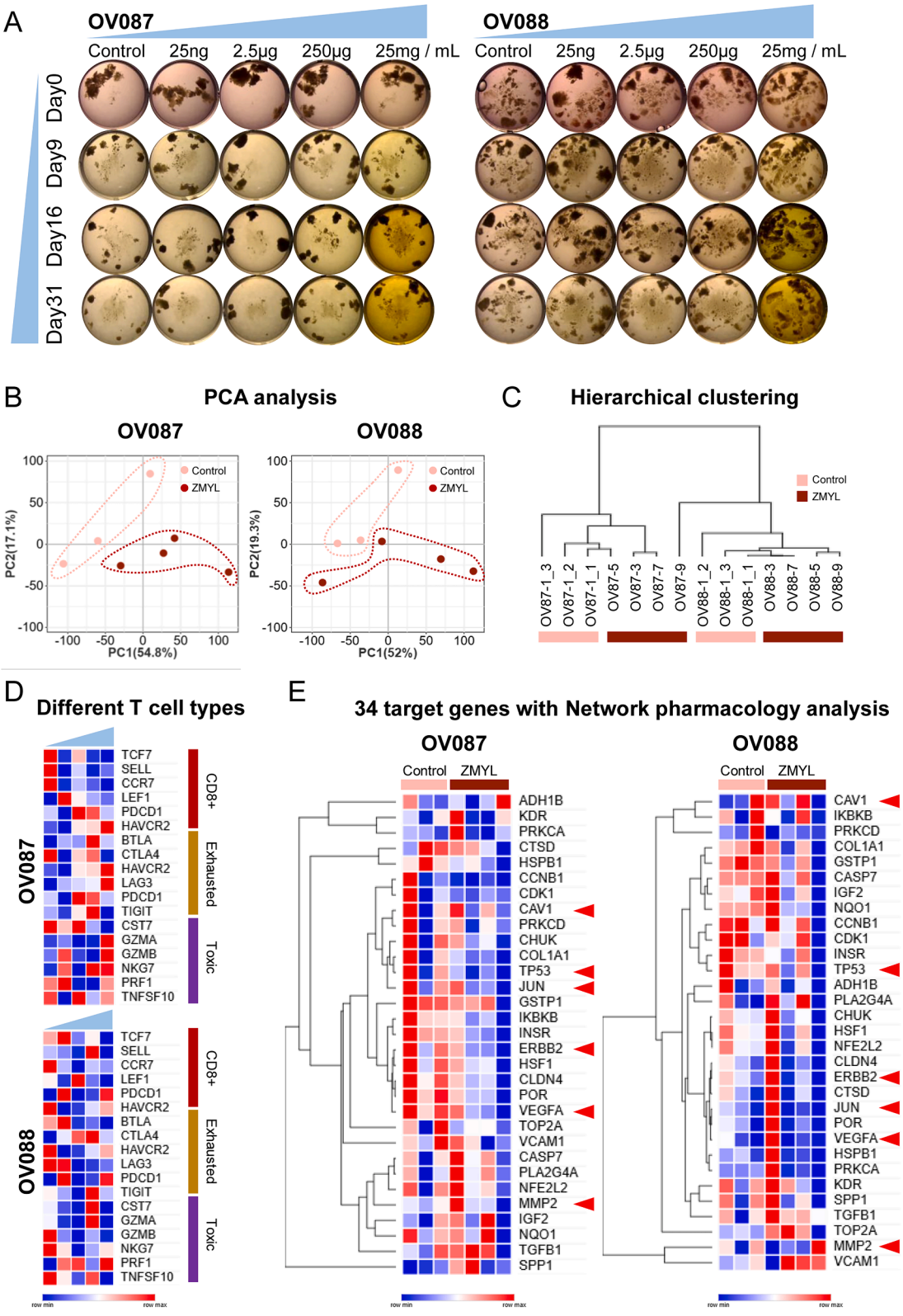

Fig. 7. Modulation of gene expression in ovarian cancer organoids by the ZMYL formula. (A) Time-lapse bright-field microscopy images of OV087 and OV088 organoids treated with the ZMYL formula at different concentrations (25 ng/mL, 2.5 μg/mL, 250 μg/mL, 25 mg/mL) and captured at various time points (Day 0, 9, 16, 31), illustrating the morphological changes. (B) PCA analysis of RNA-seq data from the treated organoids, highlighting the transcriptional variance and clustering. (C) Combined hierarchical clustering analysis of the two samples, revealing coordinated gene expression patterns. (D) Heatmap of 19 T cell related genes identified different types of T cells. (E) Heatmap of the 34 target genes identified from the network pharmacology analysis, with six genes (*TP53, JUN, VEGFA, ERBB2, MMP2, CAV1*) connected to the ZMYL formula and marked with red arrows for their significant binding interactions.

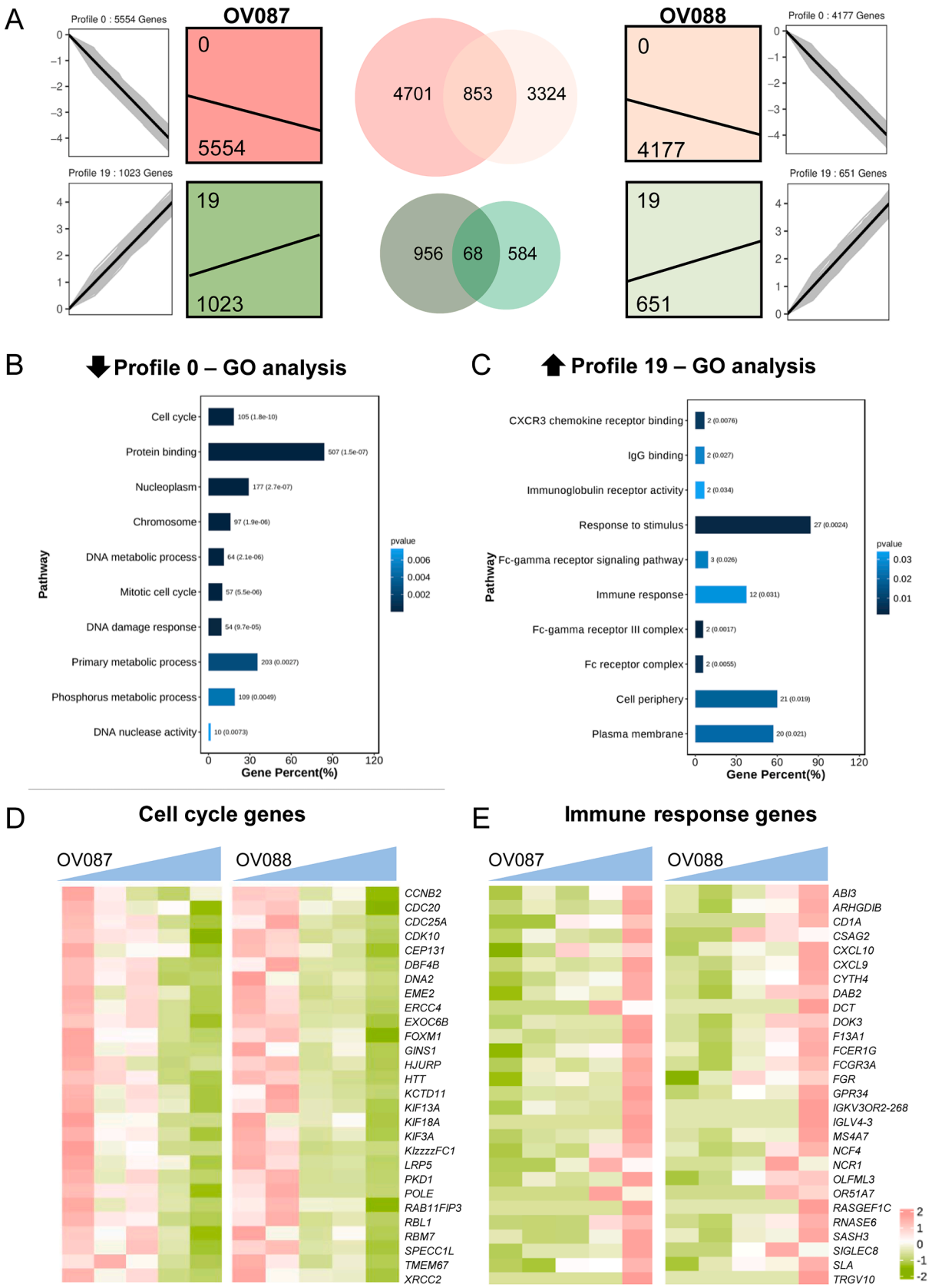

Fig. 8. Impact of ZMYL formula on immune response and cell cycle pathways in ovarian cancer organoids. (A) Trend analysis coupled with Venn diagram analysis identifies a set of 853 commonly downregulated genes and 68 commonly upregulated genes in response to increasing concentrations of the ZMYL formula. (B, C) GO analysis of the downregulated genes (profile0) suggests a suppression of cell cycle pathways, while the upregulated genes (profile19) indicate an activation of immune response pathways. (D, E) Heatmaps depict the expression of cell cycle and immune response genes in OV087 and OV088 organoids, respectively.

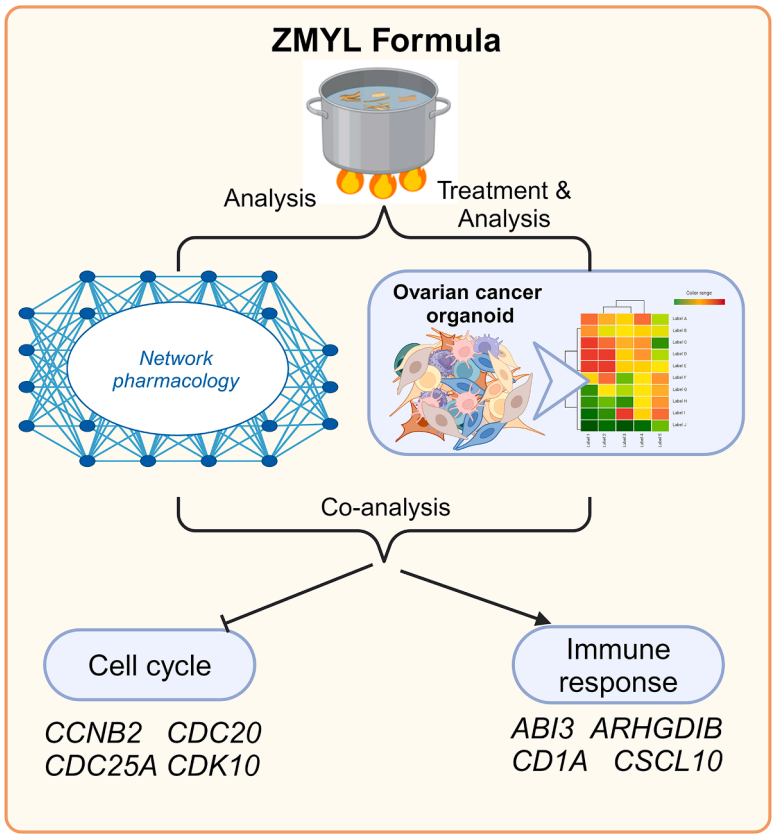

Fig. 9. Potential molecular mechanism of ZMYL formula in ovarian cancer organoids. This figure illustrates how the ZMYL formula affects ovarian cancer organoids by modulating genes in cell cycle regulation and immune response pathways, as identified through network pharmacology and transcriptomic analysis.

treatment. For example, a review of Chinese medicine's effectiveness against ovarian cancer highlights the multi-component, multi-target nature of such treatments, which is reflected in our findings (Wang et al., 2024b). The modulation of immune and cell cycle-related genes by the ZMYL formula could enhance the body's immune response against cancer cells while also targeting cell proliferation, offering a comprehensive approach to treatment.

While our study provides valuable insights into the potential of the ZMYL formula in ovarian cancer therapy, it is not without limitations. The complexity of TCM formulas and the variability in organoid responses across patients necessitate further research. Additionally, the translation of our *in vitro* findings to *in vivo* models and clinical settings is a critical next step. Despite these challenges, our work lays a solid foundation for the integration of TCM with modern oncological treatments.

Conclusion

In conclusion, our study demonstrates the potential of the ZMYL formula as a complementary therapy in ovarian cancer treatment, particularly in modulating immune responses and cell cycle progression. The integration of network pharmacology with *in vitro* organoid models offers a promising strategy for elucidating the mechanisms of action of TCM and informs future directions in cancer research and therapy.

CRediT authorship contribution statement

Qi Cao: Writing – review & editing, Writing – original draft, Methodology, Funding acquisition, Data curation, Conceptualization. **Chunhui Cai:** Writing – review & editing, Writing – original draft, Visualization, Supervision, Project administration, Methodology, Formal analysis, Data curation, Conceptualization. **Chen Wang:** Validation, Software, Methodology, Formal analysis, Data curation. **Lanyang Li:** Validation, Methodology, Data curation. **Jiping Liu:** Validation, Methodology, Investigation, Data curation. **Jian Zhang:** Visualization, Data curation. **Mingjie Rong:** Data curation. **Jiaqi Ren:** Resources. **Yanyan Han:** Resources, Data curation. **Jie Zhang:** Writing – review & editing, Writing – original draft, Visualization, Methodology, Funding acquisition, Data curation, Conceptualization. **Xinxin Han:** Writing – review & editing, Writing – original draft, Supervision, Project administration, Investigation, Conceptualization.

Declaration of competing interest

The authors declare that they have no known competing financial interests or personal relationships that could have appeared to influence the work reported in this paper.

Acknowledgments

We extend our sincere gratitude to all members of our laboratory for their invaluable contributions. This research was made possible by the generous support from the National Natural Science Foundation of China, with grant numbers 82374506 and 82174428. Additionally, we acknowledge the use of BioRender.com in crafting the diagrams for this study.

References

Amberger, J.S., Bocchini, C.A., Schiettecatte, F., Scott, A.F., Hamosh, A., 2015. OMIM.org: Online Mendelian Inheritance in Man (OMIM(R)), an online catalog of human genes and genetic disorders. Nucleic Acids Res. 43, D789–D798.

Bray, F., Laversanne, M., Sung, H., Ferlay, J., Siegel, R.L., Soerjomataram, I., Jemal, A., 2024. Global cancer statistics 2022: GLOBOCAN estimates of incidence and mortality worldwide for 36 cancers in 185 countries. CA Cancer J. Clin. 74, 229–263.

Bronger, H., Singer, J., Windmuller, C., Reuning, U., Zech, D., Delbridge, C., Dorn, J., Kiechle, M., Schmalfeldt, B., Schmitt, M., Avril, S., 2016. CXCL9 and CXCL10 predict survival and are regulated by cyclooxygenase inhibition in advanced serous ovarian cancer. Br. J. Cancer 115, 553–563.

Burley, S.K., Bhikadiya, C., Bi, C., Bittrich, S., Chen, L., Crichlow, G.V., Christie, C.H., Dalenberg, K., Di Costanzo, L., Duarte, J.M., Dutta, S., Feng, Z., Ganesan, S., Goodsell, D.S., Ghosh, S., Green, R.K., Guranovic, V., Guzenko, D., Hudson, B.P., Lawson, C.L., Liang, Y., Lowe, R., Namkoong, H., Peisach, E., Persikova, I., Randle, C., Rose, A., Rose, Y., Sali, A., Segura, J., Sekharan, M., Shao, C., Tao, Y.P., Voigt, M., Westbrook, J.D., Young, J.Y., Zardecki, C., Zhuravleva, M., 2021. RCSB Protein Data Bank: powerful new tools for exploring 3D structures of biological macromolecules for basic and applied research and education in fundamental biology, biomedicine, biotechnology, bioengineering and energy sciences. Nucleic Acids Res. 49, D437–D451.

Cao, Q., Li, L., Zhao, Y., Wang, C., Shi, Y., Tao, X., Cai, C., Han, X.X., 2023. PARPi decreased primary ovarian cancer organoid growth through early apoptosis and base excision repair pathway. Cell Transplant. 32, 9636897231187996.

Chen, X., Zhou, H., Liu, Y.B., Wang, J.F., Li, H., Ung, C.Y., Han, L.Y., Cao, Z.W., Chen, Y. Z., 2006. Database of traditional Chinese medicine and its application to studies of mechanism and to prescription validation. Br. J. Pharmacol. 149, 1092–1103.

de Witte, C.J., Espejo Valle-Inclan, J., Hami, N., Lohmussaar, K., Kopper, O., Vreuls, C.P. H., Jonges, G.N., van Diest, P., Nguyen, L., Clevers, H., Kloosterman, W.P., Cuppen, E., Snippert, H.J.G., Zweemer, R.P., Witteveen, P.O., Stelloo, E., 2020. Patient-derived ovarian cancer organoids mimic clinical response and exhibit heterogeneous inter- and intrapatient drug responses. Cell Rep. 31, 107762.

Fang, S., Dong, L., Liu, L., Guo, J., Zhao, L., Zhang, J., Bu, D., Liu, X., Huo, P., Cao, W., Dong, Q., Wu, J., Zeng, X., Wu, Y., Zhao, Y., 2021. HERB: a high-throughput experiment- and reference-guided database of traditional Chinese medicine. Nucleic Acids Res. 49, D1197–D1206.

Gong, C., Qian, L., Yang, H., Ji, L.L., Wei, H., Zhou, W.B., Qi, C., Wang, C.H., 2015a. Hepatotoxicity and pharmacokinetics of cisplatin in combination therapy with a traditional Chinese medicine compound of Zengmian Yiliu granules in ICR mice and SKOV-3-bearing nude mice. BMC Complement. Altern. Med. 15, 283.

Gong, C., Yang, H., Wei, H., Qi, C., Wang, C.H., 2015b. Pharmacokinetic comparisons by UPLC-MS/MS of isomer paeoniflorin and albiflorin after oral administration decoctions of single-herb Radix Paeoniae Alba and Zengmian Yiliu prescription to rats. Biomed. Chromatogr. 29, 416–424.

Ke, Y., Zhuang, X., You, L., 2022. Identification of core genes shared by endometrial cancer and ovarian cancer using an integrated approach. Cell Mol. Biol. 68, 140–145.

Kim, G., Jang, S.K., Ahn, S.H., Kim, S., Park, C.S., Seong, M.K., Kim, H.A., Bae, S., Lee, J. H., Kim, H., Jin, H.O., Park, I.C., 2024. Proapoptotic role of CDK1 in overcoming paclitaxel resistance in ovarian cancer cells in response to combined treatment with paclitaxel and duloxetine. Cancer Cell Int. 24, 409.

Kim, S., Chen, J., Cheng, T., Gindulyte, A., He, J., He, S., Li, Q., Shoemaker, B.A., Thiessen, P.A., Yu, B., Zaslavsky, L., Zhang, J., Bolton, E.E., 2019. PubChem 2019 update: improved access to chemical data. Nucleic Acids Res. 47, D1102–D1109.

Knox, C., Wilson, M., Klinger, C.M., Franklin, M., Oler, E., Wilson, A., Pon, A., Cox, J., Chin, N.E.L., Strawbridge, S.A., Garcia-Patino, M., Kruger, R., Sivakumaran, A., Sanford, S., Doshi, R., Khetarpal, N., Fatokun, O., Doucet, D., Zubkowski, A., Rayat, D.Y., Jackson, H., Harford, K., Anjum, A., Zakir, M., Wang, F., Tian, S., Lee, B., Liigand, J., Peters, H., Wang, R.Q.R., Nguyen, T., So, D., Sharp, M., da Silva, R., Gabriel, C., Scantlebury, J., Jasinski, M., Ackerman, D., Jewison, T., Sajed, T., Gautam, V., Wishart, D.S., 2024. DrugBank 6.0: the DrugBank Knowledgebase for 2024. Nucleic Acids Res. 52, D1265–D1275.

Kopper, O., de Witte, C.J., Lohmussaar, K., Valle-Inclan, J.E., Hami, N., Kester, L., Balgobind, A.V., Korving, J., Proost, N., Begthel, H., van Wijk, L.M., Revilla, S.A., Theeuwsen, R., van de Ven, M., van Roosmalen, M.J., Ponsioen, B., Ho, V.W.H., Neel, B.G., Bosse, T., Gaarenstroom, K.N., Vrieling, H., Vreeswijk, M.P.G., van Diest, P.J., Witteveen, P.O., Jonges, T., Bos, J.L., van Oudenaarden, A., Zweemer, R. P., Snippert, H.J.G., Kloosterman, W.P., Clevers, H., 2019. An organoid platform for ovarian cancer captures intra- and interpatient heterogeneity. Nat. Med. 25, 838–849.

Liu, Z., Guo, F., Wang, Y., Li, C., Zhang, X., Li, H., Diao, L., Gu, J., Wang, W., Li, D., He, F., 2016. BATMAN-TCM: a Bioinformatics Analysis Tool for Molecular mechANism of Traditional Chinese Medicine. Sci. Rep. 6, 21146.

Luo, Y., Xia, Y., Liu, D., Li, X., Li, H., Liu, J., Zhou, D., Dong, Y., Li, X., Qian, Y., Xu, C., Tao, K., Li, G., Pan, W., Zhong, Q., Liu, X., Xu, S., Wang, Z., Liu, R., Zhang, W., Shan, W., Fang, T., Wang, S., Peng, Z., Jin, P., Jin, N., Shi, S., Chen, Y., Wang, M., Jiao, X., Luo, M., Gong, W., Wang, Y., Yao, Y., Zhao, Y., Huang, X., Ji, X., He, Z., Zhao, G., Liu, R., Wu, M., Chen, G., Hong, L., Consortium, C., Ma, D., Fang, Y., Liang, H., Gao, Q., 2024. Neoadjuvant PARPi or chemotherapy in ovarian cancer informs targeting effector Treg cells for homologous-recombination-deficient tumors. Cell 187, 4905–4925 e4924.

Maenhoudt, N., Defraye, C., Boretto, M., Jan, Z., Heremans, R., Boeckx, B., Hermans, F., Arijs, I., Cox, B., Van Nieuwenhuysen, E., Vergote, I., Van Rompuy, A.S., Lambrechts, D., Timmerman, D., Vankelecom, H., 2020. Developing organoids from ovarian cancer as experimental and preclinical models. Stem Cell Rep. 14, 717–729.

Pinero, J., Ramirez-Anguita, J.M., Sauch-Pitarch, J., Ronzano, F., Centeno, E., Sanz, F., Furlong, L.I., 2020. The DisGeNET knowledge platform for disease genomics: 2019 update. Nucleic Acids Res. 48, D845–D855.

Qi, C., Zhang, Q.H., Li, J.X., 2012. [Effects of Zengmian Yiliu Recipe combined cisplatin on the tumor inhibition rate in platinum-resistant ovarian cancer]. Zhongguo Zhong Xi Yi Jie He Za Zhi 32, 817–821.

Qiu, P., Jie, Y., Ma, C., Chen, H., Qin, Y., Tu, K., Wang, L., Zhang, Z., 2022. Paired box 8 facilitates the c-MYC related cell cycle progress in TP53-mutation uterine corpus endometrial carcinoma through interaction with DDX5. Cell Death Discov. 8, 276.

Ru, J., Li, P., Wang, J., Zhou, W., Li, B., Huang, C., Li, P., Guo, Z., Tao, W., Yang, Y., Xu, X., Li, Y., Wang, Y., Yang, L., 2014. TCMSP: a database of systems pharmacology for drug discovery from herbal medicines. J. Cheminform. 6, 13.

Samaha, H., Pignata, A., Fousek, K., Ren, J., Lam, F.W., Stossi, F., Dubrulle, J., Salsman, V.S., Krishnan, S., Hong, S.H., Baker, M.L., Shree, A., Gad, A.Z., Shum, T., Fukumura, D., Byrd, T.T., Mukherjee, M., Marrelli, S.P., Orange, J.S., Joseph, S.K., Sorensen, P.H., Taylor, M.D., Hegde, M., Mamonkin, M., Jain, R.K., El-Naggar, S., Ahmed, N., 2018. A homing system targets therapeutic T cells to brain cancer. Nature 561, 331–337.

Senkowski, W., Gall-Mas, L., Falco, M.M., Li, Y., Lavikka, K., Kriegbaum, M.C., Oikkonen, J., Bulanova, D., Pietras, E.J., Vossgrone, K., Chen, Y.J., Erkan, E.P., Dai, J., Lundgren, A., Gronning Hog, M.K., Larsen, I.M., Lamminen, T., Kaipio, K., Huvila, J., Virtanen, A., Engelholm, L., Christiansen, P., Santoni-Rugiu, E., Huhtinen, K., Carpen, O., Hynninen, J., Hautaniemi, S., Vaharautio, A., Wennerberg, K., 2023. A platform for efficient establishment and drug-response profiling of high-grade serous ovarian cancer organoids. Dev. Cell 58, 1106–1121 e1107.

Stelzer, G., Rosen, N., Plaschkes, I., Zimmerman, S., Twik, M., Fishilevich, S., Stein, T.I., Nudel, R., Lieder, I., Mazor, Y., Kaplan, S., Dahary, D., Warshawsky, D., Guan-Golan, Y., Kohn, A., Rappaport, N., Safran, M., Lancet, D., 2016. The GeneCards Suite: from gene data mining to disease genome sequence analyses. Curr. Protoc. Bioinform. 54, 1 30 31-31 30 33.

Sun, X., Liu, Q., Huang, J., Diao, G., Liang, Z., 2021. Transcriptome-based stemness indices analysis reveals platinum-based chemo-theraputic response indicators in advanced-stage serous ovarian cancer. Bioengineered 12, 3753–3771.

Sun, Y., Li, S., Yang, L., Zhang, D., Zhao, Z., Gao, J., Liu, L., 2019. CDC25A facilitates chemo-resistance in ovarian cancer multicellular spheroids by promoting E-cadherin expression and arresting cell cycles. J. Cancer 10, 2874–2884.

Vazquez-Garcia, I., Uhlitz, F., Ceglia, N., Lim, J.L.P., Wu, M., Mohibullah, N., Niyazov, J., Ruiz, A.E.B., Boehm, K.M., Bojilova, V., Fong, C.J., Funnell, T., Grewal, D., Havasov, E., Leung, S., Pasha, A., Patel, D.M., Pourmaleki, M., Rusk, N., Shi, H., Vanguri, R., Williams, M.J., Zhang, A.W., Broach, V., Chi, D.S., Da Cruz Paula, A., Gardner, G.J., Kim, S.H., Lennon, M., Long Roche, K., Sonoda, Y., Zivanovic, O., Kundra, R., Viale, A., Derakhshan, F.N., Geneslaw, L., Issa Bhaloo, S., Maroldi, A., Nunez, R., Pareja, F., Stylianou, A., Vahdatinia, M., Bykov, Y., Grisham, R.N., Liu, Y. L., Lakhman, Y., Nikolovski, I., Kelly, D., Gao, J., Schietinger, A., Hollmann, T.J., Bakhoum, S.F., Soslow, R.A., Ellenson, L.H., Abu-Rustum, N.R., Aghajanian, C., Friedman, C.F., McPherson, A., Weigelt, B., Zamarin, D., Shah, S.P., 2022. Ovarian cancer mutational processes drive site-specific immune evasion. Nature 612, 778–786.

Wang, M., Bi, Y., Jin, Y., Zheng, Z.J., 2024a. Global incidence of ovarian cancer according to histologic subtype: a population-based cancer registry study. JCO Glob. Oncol. 10, e2300393.

Wang, Y., Xie, L., Liu, F., Ding, D., Wei, W., Han, F., 2024b. Research progress on traditional Chinese medicine-induced apoptosis signaling pathways in ovarian cancer cells. J. Ethnopharmacol. 319, 117299.

Wang, Y., Zhang, S., Li, F., Zhou, Y., Zhang, Y., Wang, Z., Zhang, R., Zhu, J., Ren, Y., Tan, Y., Qin, C., Li, Y., Li, X., Chen, Y., Zhu, F., 2020. Therapeutic target database 2020: enriched resource for facilitating research and early development of targeted therapeutics. Nucleic Acids Res. 48, D1031–D1041.

Wen, J., Xue, L., Wei, Y., Liang, J., Jia, W., Yong, T., Chu, L., Li, H., Han, S., Liao, J., Chen, Z., Liu, Y., Liu, Q., Ding, Z., Liang, H., Gan, L., Chen, X., Huang, Z., Zhang, B., 2024. YTHDF2 is a therapeutic target for HCC by suppressing immune evasion and angiogenesis through ETV5/PD-L1/VEGFA axis. Adv. Sci. 11, e2307242 (Weinh).

Yang, X., Zhou, S., Yang, C., Cao, C., He, M., Zi, S., 2022. CCNB1, negatively regulated by miR-559, promotes the proliferation, migration, and invasion of ovarian carcinoma cells. Mol. Biotechnol. 64, 958–969.

Zhang, Q.H., Gong, C., Yang, H., Wei, H., Zhou, W.B., Qi, C., Wang, C.H., 2015. Pharmacokinetics of cisplatin in the absence or presence of Zengmian Yiliu granules (a traditional Chinese medicine compound) in rats determined via ICP-MS: an investigation on drug-herb interactions. Pharm. Biol. 53, 159–166.

Zhang, S., Iyer, S., Ran, H., Dolgalev, I., Gu, S., Wei, W., Foster, C.J.R., Loomis, C.A., Olvera, N., Dao, F., Levine, D.A., Weinberg, R.A., Neel, B.G., 2021. Genetically defined, syngeneic organoid platform for developing combination therapies for ovarian cancer. Cancer Discov. 11, 362–383.

Zhao, Y., Wang, C., Deng, W., Li, L., Liu, J., Shi, Y., Tao, X., Zhang, J., Cao, Q., Cai, C., Han, X., 2024. Patient-derived ovarian cancer organoid carries immune microenvironment and blood vessel keeping high response to cisplatin. MedComm 5, e697 (2020).